Hydrodynamic impacts on tidal-scale dissolved inorganic nitrogen cycling and export across the estuarine turbidity maxima to coast

Dan Yu, Nengwang Chen, Peng Cheng, Fengling Yu & Huasheng Hong

Biogeochemistry
An International Journal

ISSN 0168-2563
Volume 151
Number 1

Biogeochemistry (2020) 151:81-98
DOI 10.1007/s10533-020-00712-4

Springer

Biogeochemistry (2020) 151:81–98
https://doi.org/10.1007/s10533-020-00712-4

Hydrodynamic impacts on tidal-scale dissolved inorganic nitrogen cycling and export across the estuarine turbidity maxima to coast

Dan Yu · Nengwang Chen · Peng Cheng · Fengling Yu · Huasheng Hong

Received: 26 July 2020 / Accepted: 21 October 2020 / Published online: 27 October 2020

Abstract Estuarine turbidity maxima (ETM) is a transition zone subject to the influence of river flow and tides. Here we showed the distinct impacts of fluvial and tidal hydrodynamics on dissolved inorganic nitrogen (DIN) cycling and export across the ETM to coast. We conducted tidal-scale hourly measurements at the ETM zone of the Jiulong River Estuary in Southeast China in May and December 2015. Generally, ammonium-N (NH_4-N) and nitrate-N (NO_3-N) increased in ebb tides, primarily controlled by freshwater input. In contrast, nitrite-N (NO_2-N) increased in flood tides, largely due to the horizontal advection of NO_2-N rich water from the middle estuary (5–10 PSU). During the fresh–saline water mixing period with high suspended particulate matters (SPM), the stronger tides and smaller river discharge in December increased SPM and NO_2-N in the ETM, indicating stronger ammonium oxidation in the water column. During the low tide period when freshwater dominated and particles were deposited, the increase of NH_4-N in the water column was related to the external source supply (e.g., wetland effluent), while the decline of NO_3-N and NO_2-N was likely associated with denitrification occurring in anoxic fluid muds and sediments. The larger DIN flux was found in May with larger river discharge, weaker tides and longer duration of the freshwater dominated period than December. This study highlights the combined effects of river and tides on hydrodynamics, which largely determine the major N sources, processes (e.g., nitrification and denitrification) and DIN fluxes across the ETM to coast.

Keywords Estuarine turbidity maxima · Dissolved inorganic nitrogen · Tidal variation · Nitrogen cycling · Land–sea interface

Introduction

Estuaries, as a transitional zone connecting rivers and the open sea, are among the most productive ecosystems in the world, due to their diverse environment with abundant nutrients (mainly nitrogen and phosphorus) derived from the watershed (Bianchi 2007). Terrestrial nutrients are utilized or transformed in estuaries before being transported to the sea (Brion et al. 2008; Erler et al. 2014; Schlarbaum et al. 2010).

Responsible Editor: Marguerite A. Xenopoulos

D. Yu · N. Chen (✉) · H. Hong
State Key Laboratory of Marine Environmental Science, Xiamen University, Xiamen 361102, China
e-mail: nwchen@xmu.edu.cn

D. Yu · N. Chen · P. Cheng · F. Yu · H. Hong
Fujian Provincial Key Laboratory for Coastal Ecology and Environmental Studies, College of the Environment and Ecology, Xiamen University, Xiamen 361102, Fujian, China

Therefore, estuaries play an important role in controlling the export of nutrients from the watershed to the sea, and this role has become more essential due to the constantly increasing nutrient loads originating from fertilizer, manure and sewage in the watershed (Damashek and Francis 2018; Erler et al. 2014; Statham 2012; Yu et al. 2015). The estuarine turbidity maxima (ETMs) are usually found at the head of the estuary where a series of hydrological and sedimentary processes cause a large sum of suspended particulate matters (SPM) to converge (Burchard et al. 2018). The ETM is highly dynamic and acts as a natural "bioreactor" for intensive transformations of nutrients (Abril et al. 2000; Owens 1986; Seitzinger et al. 2010). Nitrogen (N) is one of the key nutrients driving primary production in aquatic ecosystems, including estuaries. The high variations in N transformations and export through the ETM were mainly associated with the highly dynamic hydrology (water discharges, tidal forces) in estuaries (Hudon et al. 2017; Martin et al. 2008; Nilsson and Jansson 2002; Paudel and Montagna 2014).

Estuarine hydrology varies at different time scales, including yearly and seasonal variation of river discharges, monthly variation of tidal amplitude (spring-neap cycles) and diurnal variation of tides and currents during ebb-flood cycles (Long et al. 2013, 2018; Miguel 2018; Scully and Friedrichs 2007; Tay et al. 2012). River discharges mainly determine the magnitude of nutrient fluxes exported from the estuary to the sea (Hudon et al. 2017; Liu et al. 2009). Lower concentrations of ammonium and nitrate but higher total N loads are usually found in estuaries in wet seasons compared to dry seasons (Struyf et al. 2004; Yan et al. 2012), and others have found that the elevated discharge in wet seasons leads to decreased salinity in estuaries but no significant increases of inorganic N concentrations (Bittar et al. 2016). Seasonal variations of N concentration in river water determine the level of substrates for all N processes, while changes in river discharge can also impact the intensity of N biogeochemistry by changing the water residence time (Dettmann 2001; Martin et al. 2008; Seitzinger et al. 2006). Some studies have also investigated the spring-neap tidal contrasts on N dynamics in the lower parts of estuaries. Ammonium concentrations were found to be up to five times lower during spring tides than neap tides in a marsh-dominated estuary during the growing season, as a result of active N exchange between tidal river water and periodically-flooded marshes from neap to spring (Vorosmarty and Loder 1994). A previous study in the Jiulong River Estuary found 0.8–9.8% of the riverine ammonium was removed in the water column during or close to spring tides but 15.3–57.5% was added during or close to neap tides, which was related to the magnitude of the resuspended particles controlled by the tidal amplitude (Yu et al. 2019). On a tidal time scale, there are distinctive tidal patterns for the concentration of dissolved inorganic nitrogen (DIN), rising during the ebb flow and dropping during the flood flow (Long et al. 2013; Martin et al. 2008; Ribas-Ribas et al. 2013; Tay et al. 2012), highlighting the importance of accounting for tidal variability when estimating nutrient loading. Those observations were mostly conducted in the lower parts of the estuaries with high salinity (> 20 PSU). However, few studies have explored how tidal variations influence N cycling in the upper estuary (including ETMs).

The ETM is characterized by particle convergence and hydrological variation (Burchard et al. 2018; Doxaran et al. 2009; Uncles et al. 2002). Suspended particles, as carriers for nutrients and microorganisms, can directly or indirectly participate or affect N cycling in estuaries (Middelburg and Herman 2007; Turner and Millward 2002). Firstly, riverine particles usually contain abundant organic N (Tuduri et al. 2018). When transported to estuaries, a great proportion of those particles are trapped by the ETM and then buried in the sediment, wherein riverine organic N is gradually mineralized to ammonium. The newly produced ammonium could be nitrified in the surface sediment and released to the water column during the resuspension of sediment (Abril et al. 2000; Middelburg and Herman 2007). Secondly, the abundance and activity of microorganisms such as nitrifiers in aquatic systems are mostly particle-associated (Cottrell et al. 2010; Owens 1986; Smith et al. 2013). Strong correlations between nitrification rates and particulate concentrations have been found in many systems, likely due to the introduction of active nitrifiers from surface sediments during resuspension (Damashek et al. 2016; Frame et al. 2014). Moreover, the availability of ammonium in the water column is also affected by the balance of its adsorption–desorption on particles. The capacity for ammonium adsorption onto particles will rise when the flocculation of fine particles occurs in estuaries (Hamilton et al. 2006).

However, ammonium on particles in freshwater may desorb to the water column when freshwater meets seawater, since higher salinity reduces adsorption capacity (Percuoco et al. 2015; Rysgaard et al. 1999). While the interactions between particles and N cycling in estuaries are recognized, how hydrodynamics in the river-estuary interface impact N biogeochemical processes and fluxes are not well known.

We conducted two field observations for time-series sampling at three fixed stations in the ETM of the Jiulong River Estuary (JRE) in Southeast China in May and December 2015. The specific objectives of this study were: (1) to depict the tidal variation of suspended particles and DIN species in the ETM at the head of the estuary; (2) to explore the diverse impacts of fluvial and tidal hydrodynamics on major N sources and processes involved; and (3) to reveal the tidal driven factors regulating the flux of river DIN across the ETM to coast.

Materials and methods

Study area

The Jiulong River Estuary (JRE) is the tidal reach of the Jiulong River, which finally flows into Xiamen Bay and the Taiwan Strait in Southeast China (Fig. 1). A total of 1.47 $\times$ 10^{10} m^3 $year^{-1}$ freshwater from two major tributaries (the North River and the West River) discharges into the JRE, under the influence of the monsoon climate (Chen et al. 2018a). A third tributary (the South River) with a small discharge merges into the middle part of the estuary (Cheng et al. 2019). In the 2000s, about 61–92% of river DIN yield originated from three major anthropogenic N inputs (fertilizer, manure and sewage) and the yield reached 1662 kg N km^{-2} $year^{-1}$ for the North River, and 3097 kg N km^{-2} $year^{-1}$ for the West River (Yu et al. 2015). The semi-enclosed water body is separated by three major channels in the upper estuary, while over 90% of the freshwater travels through the southern channel of the estuary (Guo et al. 2005). JRE has a typical semidiurnal tide and is a macro tidal estuary with an average tidal range of 3.9 m. The open water area of the JRE is about 100 km^2 and the water depth in the southern channel is 3–16 m (Jiang and Wai 2005). Water temperature ranges from 13 to 32 °C and the water flushing time is about 2–3 days during normal flows (Cao et al. 2005). Along the riverbank, in the middle estuary, there are small-scale areas of mangroves dominated by *Kandelia obovate* (Chen et al. 2016). There are usually two ETMs in the JRE; one is located on the western side of Haimen Island in the upper-middle part, and the other is located on the eastern side of Jiyu Island in the lower reach (Chen et al. 2018b). In this study, we focused on the first ETM, which is strongly associated with the fresh–saline water interaction.

Sampling and laboratory analysis

Two field observations of a complete 24–25 h time-series measurement were carried out at three fixed stations (A, B, C) in the ETM of the JRE on 7th–8th May 2015 and 14th–15th December 2015 (Fig. 1).

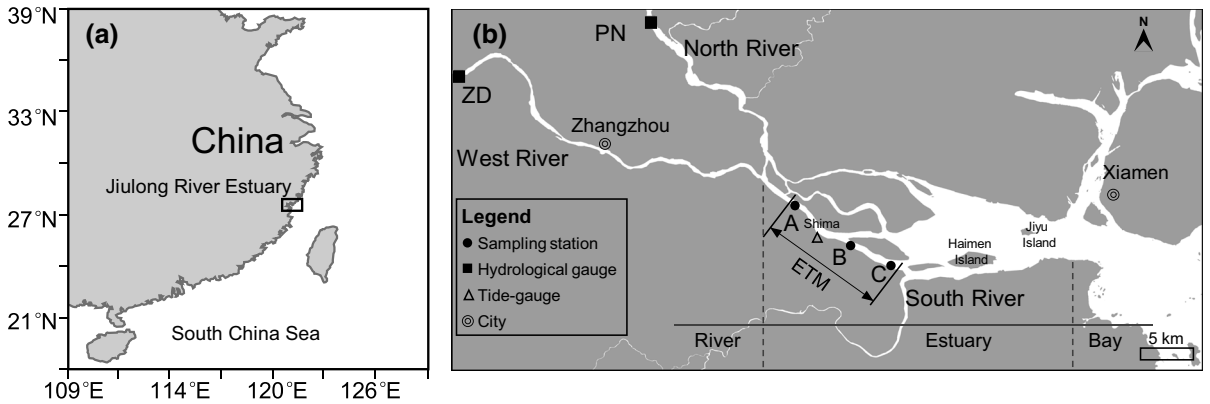

Fig. 1 Map of the estuarine turbidity maxima (ETM) in the Jiulong River Estuary showing two hydrological gauges (PN, ZD) in the river, the fixed ETM sampling sites (A, B, C), and the tide-gauge at Shima

The JRE has relatively high river discharge with weak tides in May (wet season), and relatively low discharge with strong tides in December (dry season) (Yan et al. 2012; Yu et al. 2019). In addition, before the fixed-point sampling, a background cruise measuring in-situ salinity and water temperature across the estuary was conducted to identify the fresh–saline interface and the location of the ETM. Background cruises were taken on 6th May (this data have been published by Yu et al. (2019)) and on 14th December 2015. Station A was selected in the upper ETM, station B (the key station) was in the central ETM, and station C was in the lower ETM (Fig. 1); one boat was anchored at each station. A 1200 kHz acoustic Doppler current profiler (ADCP) was mounted at station B to measure water velocity every 15 min, and these data were input to a ROMS model fitting the JRE to calculate tidal water fluxes (Cheng et al. 2019).

Surface (depth 0.5 m), middle (half of the depth) and bottom (0.5 m above the sediment surface) water samples were taken simultaneously using three self-priming pumps at station B, while only surface water was sampled by 5 L Niskin samplers at station A and station C. Water samples were collected at an interval of one hour. Portable water quality meters (WTW Multi 3430, Germany) were used to measure sample salinity, water temperature, dissolved oxygen (DO) and pH on deck. Water samples were then filtered through GF/F (0.7 μm) Whatman glass microfiber filters on the boat, and the filtrates and filters were then stored in a cool container before lab analysis at Xiamen University. A sequential filtration device (CatNet) with four nets (pore size 10, 32, 63 and 153 μm) was used for onboard filtration of size-fractioned suspended particles from a total of 5 L water at selected time points (high tide, low tide, flood tide and ebb tide). Four grain-size groups of suspended particles (> 153, 63–153, 32–63, 10–32 μm) were collected on the net and then transferred to GF/F (0.7 μm) Whatman glass microfiber filters, while the fifth group of particles (< 10 μm) were collected by filtering the residual water samples in the device on GF/F (0.7 μm) Whatman glass microfiber filters. All particulate samples were stored in cool boxes before analysis (Hsu and Liu 2010).

Filtrates were analyzed for concentrations of NO_3-N, NO_2-N and NH_4-N by a SEAL AutoAnalyzer 3 (detection limit 0.1 μmol L^{-1} for NO_3-N, 0.04 μmol L^{-1} for NO_2-N and 0.5 μmol L^{-1} for NH_4-N). DIN concentrations were a sum of NO_3-N, NO_2-N and NH_4-N; the precision was estimated by repeated determinations of 10% of the samples and the relative error was 3–5%. For quality control in the laboratory, a standard reference material provided by the National Environmental Protection Agency was used to check instrument performance, within − 1% to + 4% deviations from the standard concentrations. The total suspended particulate matters (SPM) and size-fractioned suspended particles were determined by weighting the differences between the unfiltered and filtered GF/F membranes after oven drying (105 °C) to constant weights.

Auxiliary data collection and data analysis

Daily river discharge was obtained from two hydrological stations (Punan Station in the North River and Zhengdian Station in the West River), and river discharges were extrapolated to the river mouth using the ratios of the drainage area between them. The tidal range at Shima tide-gauge was obtained from the National Marine Data & Information Service (https://www.coi.gov.cn/).

The fresh–saline water interface moved back and forth throughout the ETM of the JRE, driven by tidal cycles. Fixed stations in the ETM experienced both a riverine status (before the arrival of the fresh–saline water interface) and an estuarine status (after the arrival of the fresh–saline water interface), showing distinctive patterns of N dynamics. Therefore, according to the water salinity, we divided each tidal cycle into two periods, a fresh–saline water mixing period when salinity was larger than 0.1 PSU, and freshwater dominated period (freshwater period) when salinity was equal to or < 0.1 PSU.

Hourly fluxes of DIN species across the central ETM (station B) were estimated by multiplying the average concentration of N in the surface, middle and bottom layers and tidal water fluxes, which were calculated by the validated ROMS model (Cheng et al. 2019).

Statistical analysis

The normality of variables was assessed using the Kolmogorov–Smirnov test. One-way ANOVA was used to test the differences in the water environmental parameters between seasons, the differences in

concentrations of DIN species between the background cruises and the tidal observations.

Results

Hydrological conditions and physicochemical parameters in the ETM

Hydrological conditions and physicochemical parameters during the two cruises in 2015 are shown in Table 1. Daily river discharge ranged from 525 to 615 $m^3\ s^{-1}$ during the cruise in May in the wet season (April–September), larger than of the recorded 294–330 $m^3\ s^{-1}$ in December in the dry season (October–March). The average tidal range in the wet season was larger than in dry seasons (Yu et al. 2019). Specifically, the cruise in May was carried out around a neap tide with a tidal range of 236–266 cm, while the cruise in December around a spring tide had a tidal range of 317–345 cm.

Water temperature ranged from 24.4 to 25.6 °C in May, significantly higher than the 18.5–20.7 °C recorded in December; DO was 3.07–5.45 mg L^{-1} in May, significantly lower than the measured 5.51–7.24 mg L^{-1} in December. pH varied from 6.94 to 7.65, with no significant differences between the two cruises (Table 1).

Spatial and temporal variations of salinity and suspended particles in the ETM

In the surface water, station C (lower ETM) showed the largest variability (0.1–10.6 PSU in May and 0–11.4 PSU in December); station A (upper ETM) varied little (0–1.6 PSU in May and 0–1.7 PSU in December); and station B (central ETM) had a salinity range of 0–3.7 PSU in May and 0.1–5.2 PSU in December (Fig. 2a, c). The freshwater dominated period (Salinity $\leq$ 0.1 PSU) in the central ETM was longer than two hours, while the fresh–saline water mixing periods (Salinity $>$ 0.1 PSU) lasted 6–11 h, taking 58–83% of the 12-h tidal cycle (Fig. 3a, b).

The location of the peak value for surface SPM mostly moved with the fresh–saline water interface (around 1–2 PSU isohaline) within tidal cycles (Fig. 2b, d), and mainly occurred around the central ETM. The vertical SPM at station B ranged from 49 to 982 mg L^{-1} in May, significantly lower than of the recorded 53–4019 mg L^{-1} in December ($F = 17.19$, $p < 0.001$) (Fig. 3c, d). Higher SPM mainly occurred at 2–3 h before high tides or 1–2 h later (Fig. 3c, d), around the time when water velocities along the estuary reached up to 0.9 m s^{-1} during the flood and up to 1.2 m s^{-1} during the ebb (Fig. 3e, f); while SPM then dropped to a very low level during the freshwater period in low tides (Fig. 3c, d). Among different size groups, fine particles ($<$ 10 μm) had the highest concentration, accounting for 48–80% of the total in May and 59–82% in December (Fig. 3g–j).

Tidal variations of DIN species in the ETM

Spatial and tidal variations of DIN species in surface water across the ETM varied between different species. NH_4-N mostly decreased from the upper ETM to the lower ETM, and peaked at station B in the central ETM during low tides (Fig. 4a, d). NO_2-N had a similar spatial and temporal pattern with salinity in both seasons, and the highest concentration occurred at station C in the lower ETM during high tides (Fig. 4b, d), while in contrast the lowest concentration

Table 1 Hydrological conditions and physicochemical parameters during cruises in May and December 2015 in the ETM of the JRE

Cruise	Tidal cycle	Starting date and time	Ending date and time	Daily river discharge ($m^3\ s^{-1}$)	Tidal range (cm)	Temperature (°C)	DO (mg L^{-1})	pH
May 2015	TC1	5/7 10:00	5/7 22:00	525	236	24.5–25.6[a]	3.56–5.45[b]	7.05–7.65[a]
	TC2	5/7 22:00	5/8 10:00	615	266	24.4–24.8[a]	3.07–4.95[b]	6.94–7.40[a]
December 2015	TC1	12/14 11:00	12/14 22:00	294	345	18.8–20.7[b]	5.51–6.71[a]	7.09–7.50[a]
	TC2	12/14 22:00	12/15 10:00	330	317	18.5–19.0[b]	5.68–7.24[a]	6.99–7.39[a]

TC1 and TC2 refer to the first and the second tidal cycle, respectively. Different letters for each parameter indicate significant differences between seasons ($p < 0.05$)

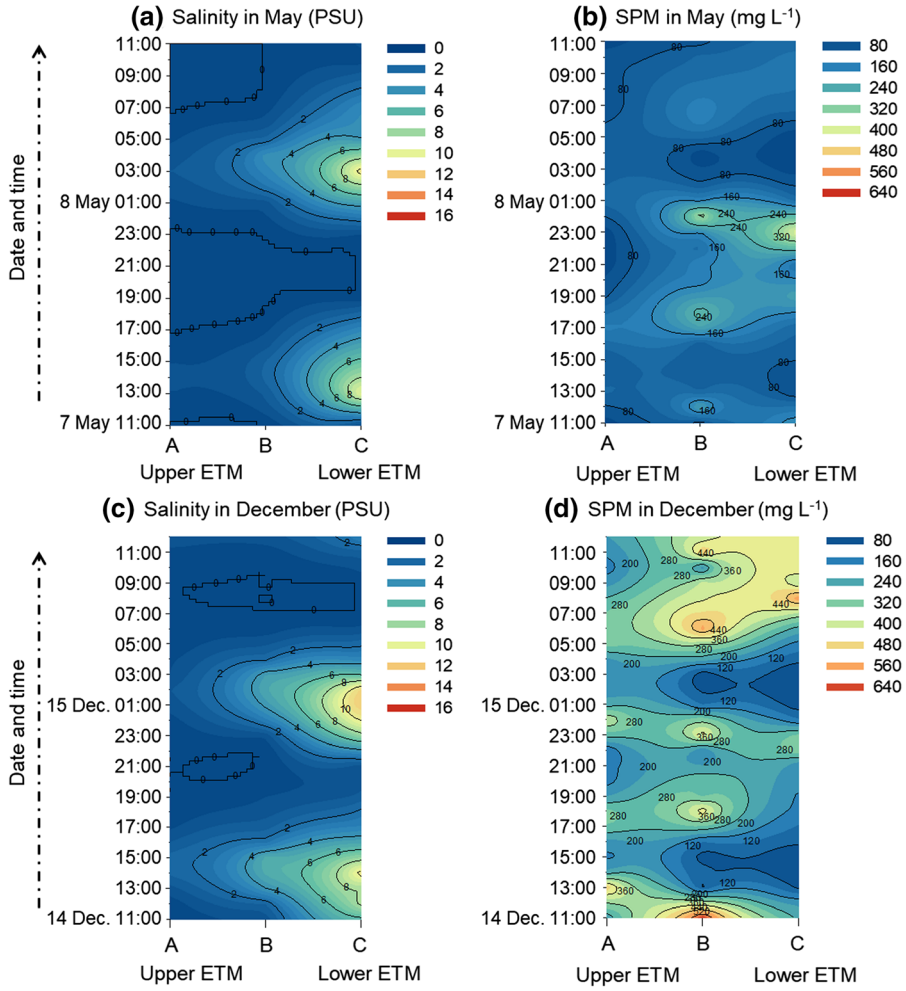

Fig. 2 Tidal variations of salinity and total suspended particulate matters (SPM) in the surface water from Station A (upper) to Station C (lower) in the ETM during tidal cycles in May and December 2015

of NO_3-N occurred at station C during high tides (Fig. 4c, f).

Nutrients at station B were found to be highly dynamic within tidal cycles but differed among species (Fig. 5). NH_4-N varied from 86.7 to 175.4 μmol L^{-1} in May, significantly higher than the recorded 48.2–70.0 μmol L^{-1} in December ($F = 92.87$, $p < 0.001$) (Fig. 5c, d). Moreover, NH_4-N was as high as 143.0–175.4 μmol L^{-1} during low tides (water depth < 5 m) in May (Fig. 5c). NO_2-N was 20.4–36.4 μmol L^{-1} in May, significantly higher than the measured 11.9–27.9 μmol L^{-1} in December ($F = 3.53$, $p < 0.001$) (Fig. 5e, f). NO_3-N was the dominant species of DIN, ranging from 149.7 to 222.9 μmol L^{-1} in May and from 224.2 to 281.2 μmol L^{-1} in December (Fig. 5g, h).

DIN significantly varied during the freshwater dominated period in low tides (Fig. 5), and their concentration changes (differences) to the start point of freshwater periods were calculated (Fig. 6). NH_4-N was significantly higher during these periods in May (up to 42.8 ± 4.6 μmol L^{-1} in TC1 and 22.8 ± 6.7 μmol L^{-1} in TC2) (Fig. 6a), but was much lower (up to 3.1 ± 0.8 μmol L^{-1}) in December (Fig. 6b). Changes in NO_2-N were relatively small (the lowest was − 3.4 ± 0.1 μmol L^{-1} in TC2 in December and the highest was 1.4 ± 0.3 μmol L^{-1} in TC2 in May) (Fig. 6c, d). NO_3-N increased by 9.6 ± 9.2 μmol L^{-1} in TC1 in May but was lowered

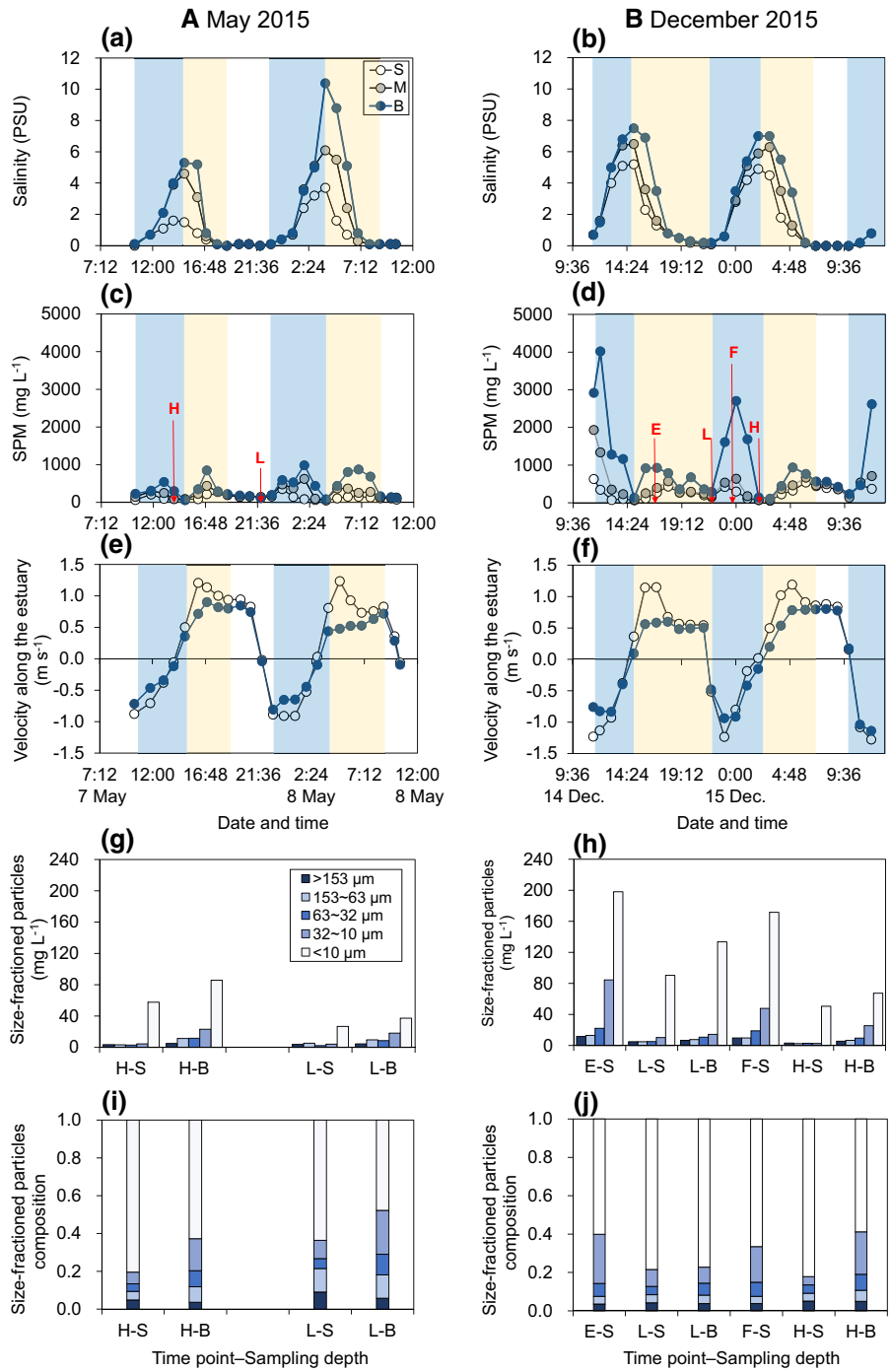

Fig. 3 Tidal variations of salinity (**a**, **b**), total suspended particulate matters (SPM) (**c**, **d**), size-fractioned particles (**e**, **f**) and their compositions (**g**, **h**) in the central ETM (Station B) of the JRE in May and December 2015. The colored background refers to the fresh–saline water mixing period (blue represents flood tides, light yellow represents ebb tides), and the remainder refers to the freshwater period. *S* surface water; *M* middle water; *B* bottom water; *H* high tide; *L* low tide; *F* flood tide; *E* ebb tide. (Color figure online)

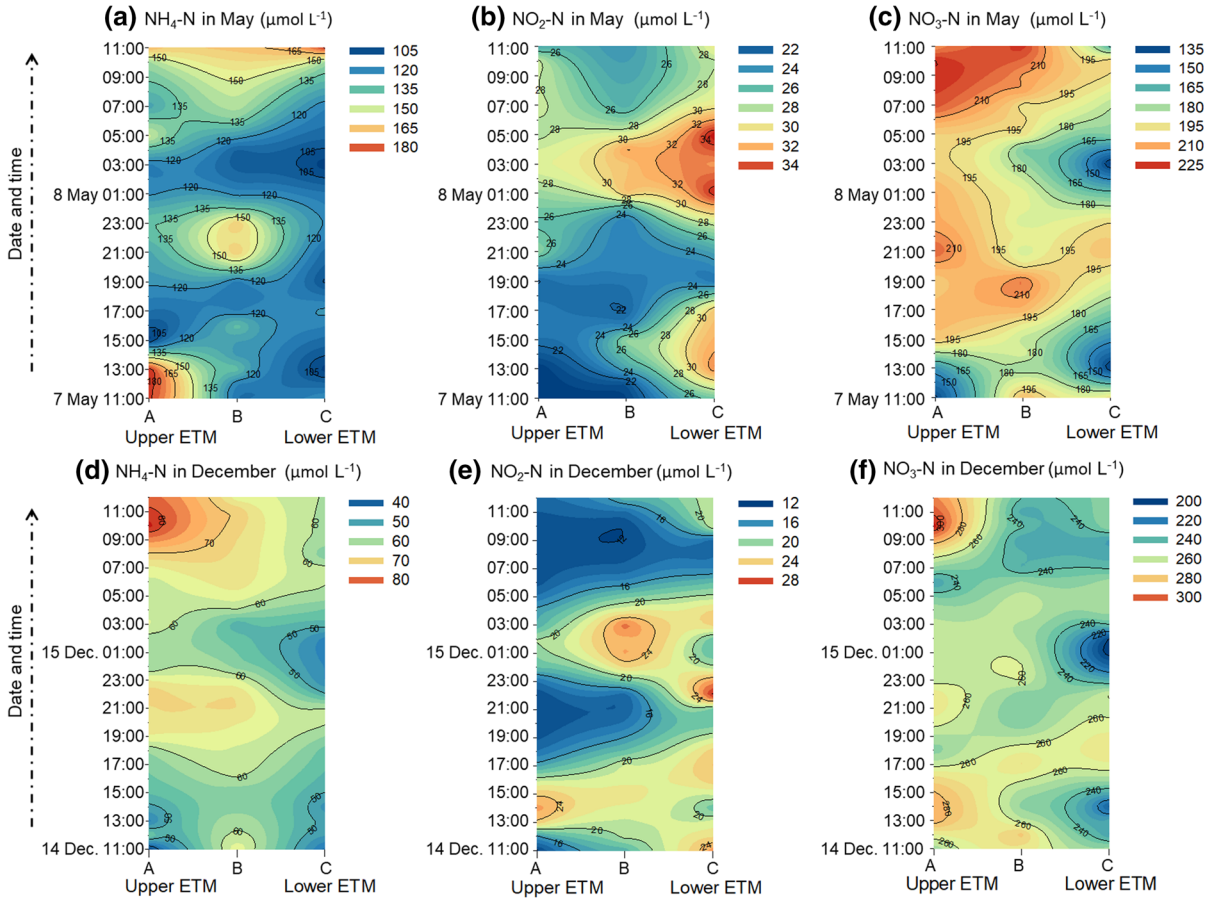

Fig. 4 Tidal variations of NH_4-N, NO_2-N and NO_3-N in the surface water from Station A (upper) to Station C (lower) across the ETM during tidal cycles in May and December 2015

by 18.6 ± 3.1 μmol L^{-1} in TC2 in May and by 9.3 ± 2.1 μmol L^{-1} in TC2 in December (Fig. 6e, f).

Relationship between DIN species and salinity during fresh–saline water mixing periods in the central ETM

The relationship between nutrient concentration and salinity is often used to identify the patterns of addition or removal of nutrients during the mixing of freshwater and seawater end-members. In the present study, we compared the N-salinity pattern at station B to that in the background cruises during the fresh–saline water mixing period.

NH_4-N versus salinity curves in the two background cruises were above the mixing line. NH_4-N in tidal observations in May was significantly lower than that in its background cruise ($F = 8.764$, $p < 0.01$) (Fig. 7a, b), whereas there was no significant difference between the observations in December ($F = 2.245$, $p > 0.05$) (Fig. 7c, d). NO_2-N versus salinity in the two background cruises were above the mixing lines. NO_2-N in tidal observations in both seasons fitted their background curves well (Fig. 7e–h), with no significant differences between the tidal observations and the background cruises ($F = 0.167$, $p > 0.05$ for May; $F = 1.737$, $p > 0.05$ for December). NO_3-N versus salinity curves in the background cruises were above the mixing lines, especially in December (Fig. 7i–l), and there was no significant difference between the tidal observations and the background cruises in May ($F = 0.113$, $p > 0.05$), while NO_3-N in the tidal observations was significantly lower than that in the background cruise in December ($F = 13.161$, $p < 0.01$).

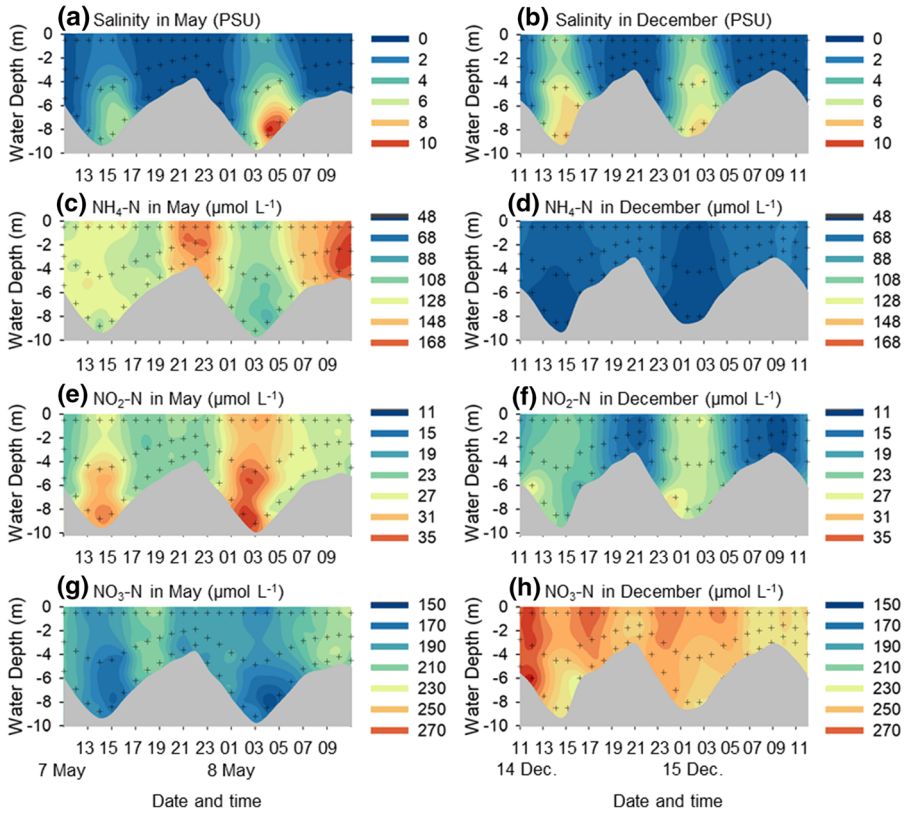

Fig. 5 Tidal variations of salinity, NH_4-N, NO_2-N and NO_3-N in the central ETM (Station B) of the JRE in May and December 2015. " + " shows the sampling location every hour

To quantify the addition or removal of DIN during the fresh–saline water mixing periods in each tidal cycle, the maximum N offset (difference) between the N-salinity curves and the background mixing line was calculated (Table 2). The maximum N offset of NH_4-N and NO_3-N in December account for − 3.1 to 6.7% and 14.8–15.4% of their background riverine N, respectively. The maximum N offsets for NO_2-N in May (81.4–98.0%) were lower than that in December (112.3–136.7%).

Tidal fluxes of DIN species

Over 24 h (two tidal cycles), the tidal fluxes of all DIN species across the ETM (station B) in May were much larger than those in December (Table 3). The 24-h tidal flux of DIN in May was 176.7 tons N per day seaward but was only 60.7 tons N per day seaward in December. An amount of 40.6 tons of NH_4-N was exported seaward during the 4-h freshwater dominated period in TC1 in May, comprising 90% of the total fluxes of 45.1 tons per tidal cycle. However, the 2-h freshwater dominated period in TC2 in May exported only 18.6 tons of NH_4-N (77% of a total of 24.2 tons). NO_2-N made the smallest contribution to tidal N fluxes, comprising < 5% of the DIN flux. As for NO_3-N, 6.5–12.8 tons were exported seaward during the fresh–saline water mixing periods in May, while 2.5–3.3 tons were imported landward during the same periods in December.

Discussion

Tidal variation revealed different sources of N species in the ETM

Hourly measurements revealed distinctive patterns of tidal transition among DIN species, implying that their source end-members varied over tidal mixing cycles. NH_4-N and NO_3-N decreased as the water level rose and increased as the water level fell (Fig. 5), primarily

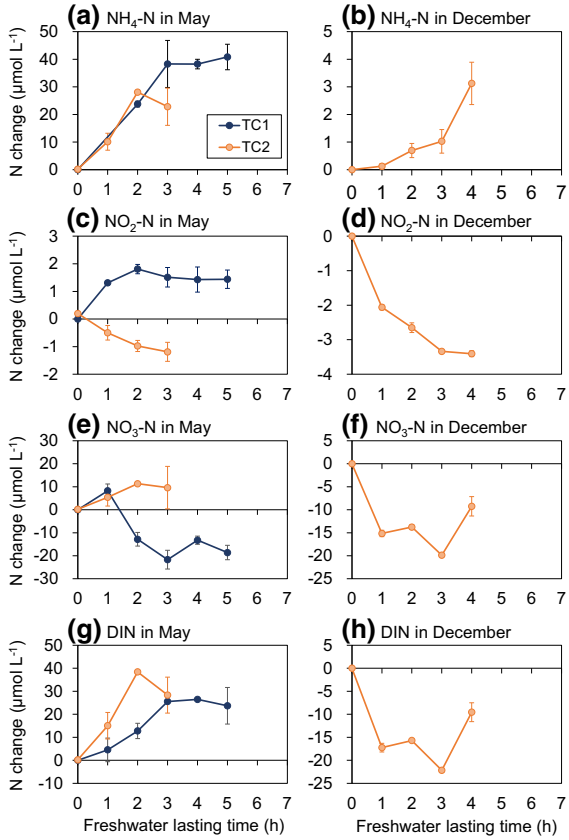

Fig. 6 Nitrogen concentration change during the freshwater periods in the central ETM (Station B) of the JRE in May and December 2015. Data indicate the average concentration with a standard deviation of three layers at each time point. TC1 and TC2 denote the first and the second tidal cycle, respectively. The freshwater period in TC1 in December was excluded since it lasted < 2 h

controlled by the input of riverine NH_4-N and NO_3-N. In the Hackensack River estuary in the US, NH_4-N was found to increase as the water level fell with a lag of 1 h in the lower estuary over semidiurnal periods, primarily affected by horizontal advection and point source loadings (DiLorenzo et al. 2004). In Sado estuary in Portugal, NO_x (nitrate plus nitrite) increased during flood tides and reached peak values 2–3 h after high tides, likely influenced by upwelling NO_x enriched water (Goncalves et al. 2015). NH_4-N and NO_3-N were also higher in low tides than high tides in two shallow tidally dominated estuaries in New Zealand (Tay et al. 2012). However, we found that NO_2-N increased as water level rose (flood tides) and peaked 1–2 h before high tides (Fig. 5). Sediments could be a potential source supply of nitrite to the water column. However, nitrite in sediment is usually very low or even undetectable (Mortimer et al. 1999). Moreover, the peak of nitrite occurred during high tides when there were few resuspended sediments and the least potential to release a large amount of nitrite (Figs. 3, 5). Therefore, we concluded that the high NO_2-N in the ETM mostly derived from enriched NO_2-N water in the middle estuary with salinity around 5–10 PSU, as previously reported by Yu et al. (2019).

The seasonal comparison allowed further identification of other N sources. NH_4-N increased by 42.8 ± 4.6 μmol L^{-1} during tidal cycles in May (Fig. 6a), but by only 3.1 ± 0.8 μmol L^{-1} in December (Fig. 6b). Wastewater discharge could contribute to the large increase of NH_4-N but there should be little seasonal difference (DiLorenzo et al. 2004), suggesting that there should be some other N sources in the JRE with distinctive seasonal differences. There are mangroves and salt marsh fringes along the middle JRE (Chen et al. 2016), and due to the enrichment of organic matter and anoxic conditions in mangrove and salt marsh sediments, there would be ample ammonium accumulated in the sediment (porewater) through the degradation of organic matter by ammonification (Reef et al. 2010). A large stock of ammonium (1–22 mg NH_4-N per kg sediment) has been found in the mangrove sediments of the JRE (Chen et al. 2015), and part of this ammonium could be exported to the estuary via subsurface runoff, which is driven by the increasing hydraulic gradient in the ebb and low tides (Santos et al. 2012; Wilson and Morris 2012). The previous studies showed that there was a larger ammonium stock in sediments in spring and summer than in winter, largely due to stronger mineralization of organic matter in warm seasons (Chen et al. 2015; Wang et al. 2019). Hence, we speculated that this might explain the larger addition of ammonium in May than December during the freshwater period in this study.

Non-conservative behaviors of each species of DIN during the mixing of two significant steady-state end-member components were usually identified by analysis of the relationship between N concentrations and salinity, and this could also be used to check the temporal variability of end-members by examining how constituent-salinity curves change with time. As modeled by Loder and Reichard (1981), for riverine nutrient variability within a period less than the

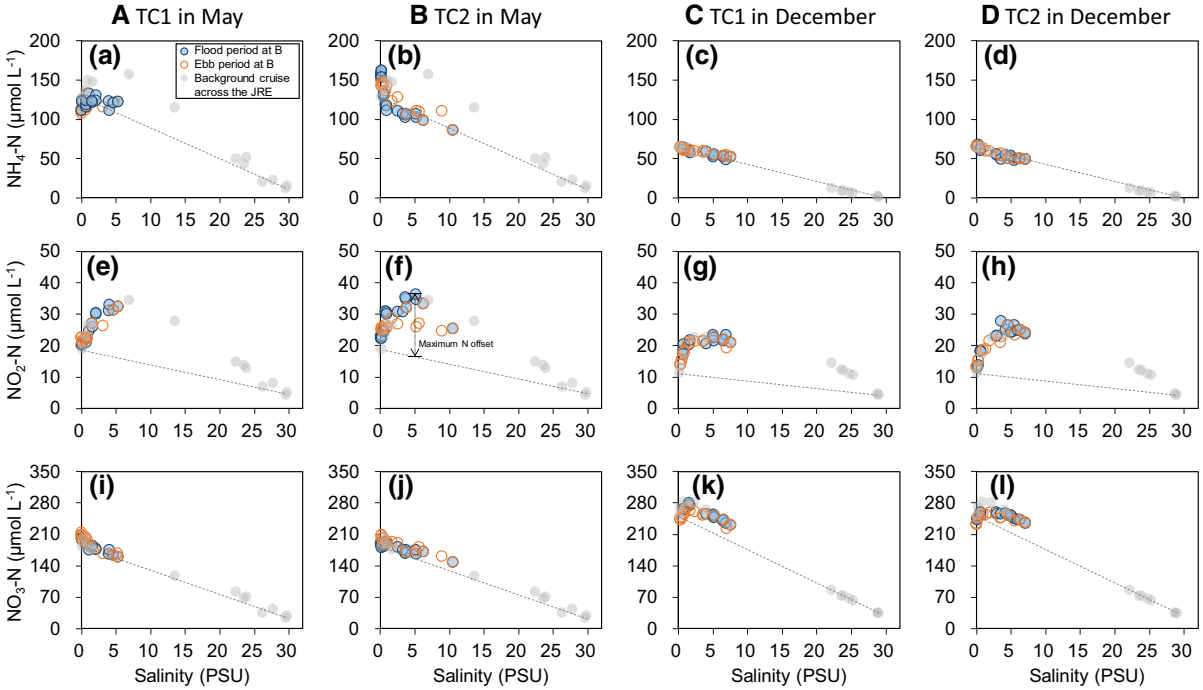

Fig. 7 Relationship between concentrations of DIN species and salinity in the central ETM (Station B) in two successive tidal cycles during fresh-saline water mixing periods in May and December 2015. TC1 and TC2 denote the first and the second tidal cycle, respectively. Dashed lines refer to the conservative mixing lines in the background cruises along the river-estuary gradient before the fixed-station observation

Table 2 Maximum nitrogen offset during fresh–saline water mixing periods in the ETM of the JRE

Cruise	N species	Maximum N offset (μmol L^{-1})		Maximum N offset/background riverine N (%)	
		TC1	TC2	TC1	TC2
May 2015	NH_4-N	/	/	/	/
	NO_2-N	15.5	18.7	81.4	98.0
	NO_3-N	/	/	/	/
December 2015	NH_4-N	− 2.0	− 4.4	− 3.1	− 6.7
	NO_2-N	12.9	15.7	112.3	136.7
	NO_3-N	38.8	37.3	15.4	14.8

The maximum N offset is the maximum concentration difference between the observed tidal N concentration and the mixing line in the background cruise at the same salinity. Positive N offset represents nitrogen addition and negative offset represents nitrogen removal. TC1 and TC2 refer to the first and the second tidal cycle, respectively. A slash indicates the maximum N offset was not able to be appropriately determined because the concentration versus salinity curve was partly above and partly around the background mixing line

flushing time, the increasing of riverine constituents would lead to a downwards-bending curve (concave shape), whereas the decreasing of riverine constituents would lead to an upwards-bending curve (convex shape). A previous study showed that the maximum daily NH_4-N variation was about 5 μmol L^{-1} at the outlet of the North Jiulong River (Ma et al. 2018), $< 10\%$ of the NH_4-N concentration in the ETM when free of storm influence. However, storm events would raise DIN by a factor of 1.5–2.0 in 24 h in the Jiulong River (Wu 2015). In the present study, the 12-h sampling timescale in each tidal cycle at the fixed

Table 3 Tidal fluxes of DIN species across the ETM to coast in May and December 2015

N species	Tidal cycle	May 2015		December 2015	
		Period	Flux (ton N)	Period	Flux (ton N)
NH_4-N	TC1	Fresh–saline (8 h)	4.2	Fresh–saline (11 h)	2.6
		Freshwater (4 h)	40.9	Freshwater (1 h)	0.3
		12 h	45.1	12 h	2.9
	TC2	Fresh–saline (10 h)	5.6	Fresh–saline (9 h)	2.4
		Freshwater (2 h)	18.6	Freshwater (3 h)	13.8
		12 h	24.2	12 h	16.1
	TC1 + TC2	24 h	69.3	24 h	19.0
NO_2-N	TC1	Fresh–saline (8 h)	0.1	Fresh–saline (11 h)	− 1.7
		Freshwater (4 h)	6.7	Freshwater (1 h)	0.1
		12 h	6.8	12 h	− 1.6
	TC2	Fresh–saline (10 h)	− 1.8	Fresh–saline (9 h)	− 2.0
		Freshwater (2 h)	2.9	Freshwater (3 h)	2.5
		12 h	1.1	12 h	0.5
	TC1 + TC2	24 h	7.9	24 h	− 1.2
NO_3-N	TC1	Fresh–saline (8 h)	12.8	Fresh–saline (11 h)	− 2.5
		Freshwater (4 h)	55.5	Freshwater (1 h)	0.9
		12 h	68.2	12 h	− 1.6
	TC2	Fresh–saline (10 h)	6.5	Fresh–saline (9 h)	− 3.3
		Freshwater (2 h)	24.8	Freshwater (3 h)	47.8
		12 h	31.3	12 h	44.5
	TC1 + TC2	24 h	99.5	24 h	42.9
DIN	TC1	Fresh–saline (8 h)	17.1	Fresh–saline (11 h)	− 1.6
		Freshwater (4 h)	103.0	Freshwater (1 h)	1.2
		12 h	120.1	12 h	− 0.4
	TC2	Fresh–saline (10 h)	10.4	Fresh–saline (9 h)	− 3.0
		Freshwater (2 h)	46.2	Freshwater (3 h)	64.1
		12 h	56.6	12 h	61.1
	TC1 + TC2	24 h	176.7	24 h	60.7

TC1 and TC2 refer to the first and the second tidal cycle, respectively. Positive value refers to seaward fluxes and negative value refers to landward fluxes

stations was shorter than the estuary flushing time of (2–3 days). Therefore, we carefully compared the N-salinity curves obtained from the tidal observations with those along the whole river-estuary gradient in the background cruise (Fig. 7).

NH_4-N in the tidal observations was significantly lower than that in the background cruise in May ($p < 0.01$) (Fig. 7a), suggesting the N-salinity curve bent downward (concave shape) caused by increasing riverine NH_4-N input or less NH_4-N addition during the tidal mixing processes. However, in December, the NH_4-N curve was close to the mixing line, and there was no significant difference between the tidal observations and the background cruise ($p > 0.05$), indicating little variation of riverine NH_4-N during the 24-h observation. There were rains in the Jiulong River watershed a few days before the cruise in May (Yu et al. 2019). The "flush effect" of storm runoff might cause large fluctuation of riverine ammonium (Chen et al. 2012, 2018a), which could be reflected by the downward-bending NH_4-N versus salinity curves. In contrast, river nitrate, the dominated DIN species,

mainly originates from groundwater so it is relatively stable in storm runoff (Chen et al. 2012). In the present study, there was no difference in the NO_3-N curve between the background cruises and the tidal observations in May ($p > 0.05$), suggesting that nitrate was more stable and its variation in river end-member was too small to be observed. Although the cruise in December was free of storm influence, NO_3-N in the tidal observations was significantly lower than that in the background cruise ($p < 0.01$), likely due to stronger nitrate removal than addition processes (e.g., denitrification and nitrification).

Impacts of fluvial and tidal hydrodynamics on N cycling in the ETM

NO_2-N versus salinity curves in all tidal observations fitted well with their background curves (Fig. 7e–h), and there was no significant difference between them ($p > 0.05$), suggesting little variability of NO_2-N in river end-member during the 24-h observations, even under the influence of storm runoff in May. This finding indicates that the NO_2-N curves at fixed stations in each tidal cycle can be used to examine nitrite behavior and associated processes. The NO_2-N versus salinity curves in the two background cruises looked convex above the mixing lines, indicating NO_2-N addition in the upper estuary (Fig. 7e, g).

Significant NO_2-N addition was observed in May and December (Table 2). NO_2-N accumulation could be found resulting from nitrate reduction to nitrite by some phytoplankton species in other aquatic systems (Naik and Chen 2008; Zakem et al. 2018), but this process should be limited in the turbid ETM zone where the primary productivity is usually low (Yan et al. 2019). Although DO in the water column was significantly lower in May than in December, it was still above the hypoxia threshold (Table 1). Considering the abundant ammonium and sufficient oxygen, the water column of the JRE in both seasons was an ideal place for nitrification. The higher ammonium concentration in May was supposed to support higher nitrification in the water column (Damashek et al. 2016). However, higher ammonium removal and higher nitrite and nitrate addition was found in December than in May, which might indicate ammonium was not a limiting factor for nitrification in the water column in JRE. As found in previous studies, the accumulation of NO_2-N in the JRE could be largely attributed to the fact that the ammonium oxidation rate is 10–20 times faster than the nitrite oxidation (Yan et al. 2019; Yu et al. 2019). Water temperature is one of the important factors affecting nitrification rates (Dai et al. 2008), and water temperature in the JRE in this study was 18–26 °C (Table 1), falling in the range at which decoupling of the ammonium-oxidation and nitrite-oxidation occurred resulting in nitrite accumulation (Schaefert and Hollibaugh 2017). Previous studies have suggested that the intensity of nitrite addition is related to a certain range of SPM, which could affect the abundance of nitrifying bacteria attached to particles (Abril et al. 2000; Luo et al. 2014). In this study, there was also apparent nitrate addition (14.8–15.4%) in December corresponding with higher SPM, compared with May when there was no apparent nitrate addition and lower SPM (Fig. 3 and Table 2). Higher SPM in December was mainly caused by stronger tides and sediment resuspension (Fig. 3). Here we found that strong tides tend to strengthen nitrification, resulting in ammonium removal and nitrite accumulation in the water column of ETM.

Moreover, NO_2-N and NO_3-N were found to decline during freshwater periods (Fig. 6). The loss of NO_2-N and NO_3-N were likely associated with processes such as denitrification or phytoplankton assimilation, which might have occurred somewhere in the ETM. During the flood and ebb tides, a large amount of all size-fractioned sedimentary particles (dominated by fine particles) were scoured and suspended into the overlying water, a great proportion of which subsequently settle down over slack-water periods in low tides (Fig. 3). Massive sediments deposition (especially of fine particles) in estuaries often creates fluid mud (a flowing mixture of mud and water), resulting in an anoxic environment and speeding up denitrification process and N removal (Abril et al. 2000, 2010; McAnally et al. 2007; Uncles et al. 2006). In the present study, we did not measure the fluid mud directly as samples were taken from the surface to 0.5 m above sediments. Nevertheless, significant denitrification end-products (excess N_2) in the upper JRE was observed earlier (Wu et al. 2013). Moreover, considering the high ammonium concentration during this period, nitrate and nitrite assimilation would not be a major process since phytoplankton commonly prefer utilizing ammonium N (Glibert and McCarthy 1984). Therefore, we speculated that the

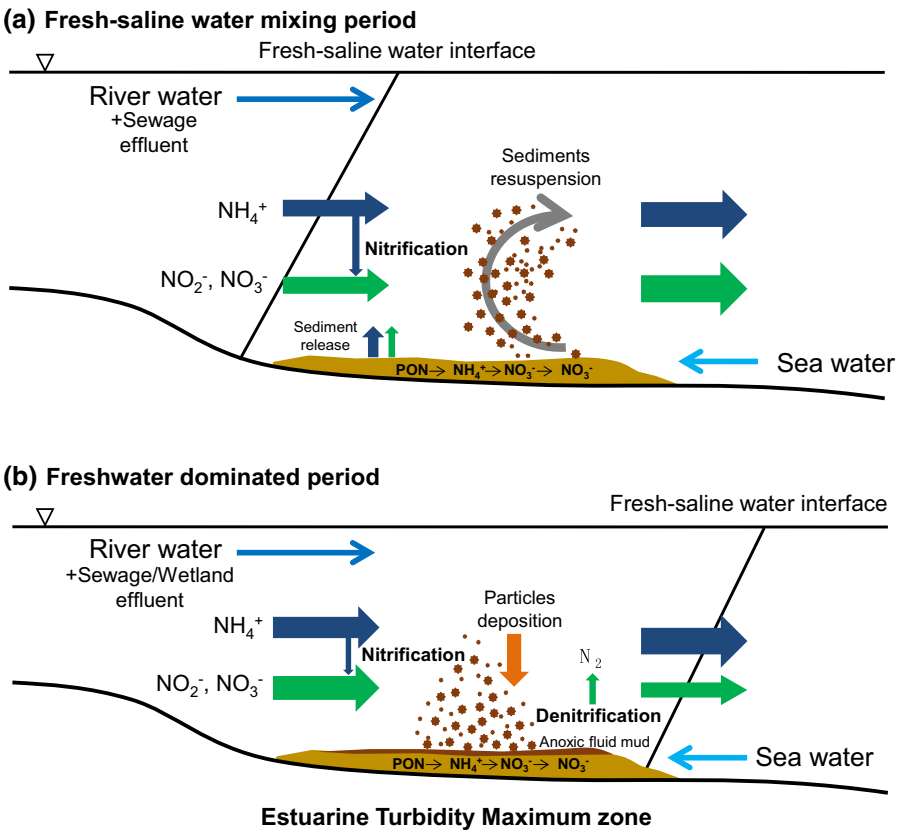

Fig. 8 A conceptual schematic of hydrodynamic impacts on tidal-scale dissolved inorganic nitrogen cycling and export across the estuarine turbidity maximum zone

decline of NO_2-N and NO_3-N in low tides very likely resulted from stronger denitrification in the fluid mud during freshwater periods.

Tidal driven exports of DIN species across the ETM to coast

The 24-h tidal fluxes of DIN in May were 1.3–5.7 times larger than those in December (Table 3), corresponding to the larger river flow in May (525–615 $m^3\ s^{-1}$) than in December (249–330 $m^3\ s^{-1}$) (Table 1), indicating the major control of river discharge over the magnitude of N fluxes. The higher NH_4-N and NO_2-N in May also contributed to their higher tidal fluxes (Fig. 5). Within tidal cycles, the freshwater dominated period exported the majority of DIN from the central ETM to coast, as 74–86% of NH_4-N and 81–114% of NO_3-N was exported (Table 3). Moreover, the larger DIN seaward fluxes were associated with the longer duration of the freshwater dominated period and smaller tidal range during weak tides (Table 3). It has been found that tidal asymmetry could cause a net seaward flux of DIN (nitrate plus ammonium) per tidal cycle in tidally dominated estuaries in New Zealand (Tay et al. 2012). Therefore, in a tidally dominated estuary like the JRE, a higher proportion of DIN is exported from the ETM to the sea during weak tides than strong tides. Extra NH_4-N inputs from the nearby wetland and wastewater discharge in low tides were also important contributions to the tidal DIN fluxes.

Although N fluxes during fresh–saline water mixing periods were relatively small, they were still important, especially for tidal cycles where the freshwater dominated period had a short duration, like TC1 in December (Table 3). About 2.6 tons of NH_4-N was exported seaward during the 11-h fresh–saline water mixing period in TC1, taking around 90% of the 12-h tidal flux, while the NH_4-N flux during the 9-h fresh–saline water mixing period in TC2 only accounted for 15% of the 12-h tidal flux. Net tidal DIN fluxes during the fresh–saline water mixing period were the net fluxes between the flood period (landward fluxes) and the ebb period (seaward fluxes). Therefore,

the larger water fluxes and DIN concentrations during ebb periods than flood periods cause more seaward export of DIN within tidal cycles. Then, the competition between DIN addition and removal between flood and ebb periods would also impact the net tidal DIN fluxes. Theoretically, stronger DIN addition during ebb periods than flood periods would lead to more seaward DIN exports.

Conclusions

The high-resolution measurements conducted in this study revealed a distinctive tidal transition pattern of DIN species in the ETM of the JRE, as summarized in the conceptual schematic (Fig. 8). Our results reflected different end-member sources and processes involved in the river-estuary system at tidal cycle timescale. The ETMs played critical roles in regulating N cycling. During the fresh–saline water mixing period with high SPM, the stronger tide and smaller river discharge in December increased SPM and nitrite in the ETM, indicating stronger nitrification (ammonium oxidation) occurred in the water column. During the low tide period when freshwater dominated and SPM was deposited, the increase of NH_4-N in the water column was related to supply from external sources (e.g., wetland effluent), while the decline of nitrate and nitrite was likely associated with denitrification occurring in anoxic fluid muds and sediments. NH_4-N and NO_3-N always increased in the ebb tide, primarily controlled by freshwater input. There was larger DIN export to coast in May, when there was a larger river discharge, weaker tide and longer duration of the freshwater dominated period compared to December. Extra NH_4-N inputs from the nearby wetlands and wastewater discharge in low tides were also important contributors to the tidal DIN fluxes. Current results suggested the combined impacts of fluvial and tidal hydrodynamics on estuarine N sources, behaviors, and associated processes and fluxes across the ETM to coast. However, more observations, modeling and system integration works are needed to further understand the mechanisms controlling nutrient delivery from land to ocean.

Acknowledgements This study was supported by the National Natural Science Foundation of China (No. 41676098), Fujian Environmental Protection Science and Technology Project (No. 2018R007), and Fundamental Research Funds for the Central Universities (No. 20720180119). Peng Cheng acknowledges funding from the National Natural Science Foundation of China (No. 41476004). Fengling Yu acknowledges funding from the Youth Program of National Natural Science Foundation of China (No. 41706039). We thank CEES Open Cruise for Jiulong River Estuary—Xiamen Bay and Shuiying Huang for her organization. We also thank the crew and all the students at Xiamen University on R/V Ocean II for their assistance in the cruises.

Funding National Natural Science Foundation of China (Nos. 41676098; 41476004; 41706039); Fujian Environmental Protection Science and Technology Project (No. 2018R007); Fundamental Research Funds for the Central Universities (No. 20720180119).

Data availability The data presented in this manuscript are original and will be available in the repository (https://47.105.173.165:8008/MIS/File_Upload.jsp, Marine Monitoring and Information Service Center, Xiamen University) by acceptance.

Code availability Not applicable.

Compliance with ethical standards

Conflict of interest The authors declare that they have no conflict of interest.

References

Abril G, Riou SA, Etcheber H, Frankignoulle M, de Wit R, Middelburg JJ (2000) Transient, tidal time-scale, nitrogen transformations in an estuarine turbidity maximum—fluid mud system (The Gironde, South-west France). Estuar Coast Shelf Sci 50:703–715. https://doi.org/10.1006/ecss.1999.0598

Abril G, Commarieu MV, Etcheber H, Deborde J, Deflandre B, Zivadinovic MK, Chaillou G, Anschutz P (2010) In vitro simulation of oxic/suboxic diagenesis in an estuarine fluid mud subjected to redox oscillations. Estuar Coast Shelf Sci 88:279–291. https://doi.org/10.1016/j.ecss.2010.04.003

Bianchi TS (2007) Biogeochemistry of estuaries. Oxford University, Demand

Bittar TB, Berger SA, Birsa LM, Walters TL, Thompson ME, Spencer RGM, Mann EL, Stubbins A, Frischer ME, Brandes JA (2016) Seasonal dynamics of dissolved, particulate and microbial components of a tidal saltmarsh-dominated estuary under contrasting levels of freshwater discharge. Estuar Coast Shelf Sci 182:72–85. https://doi.org/10.1016/j.ecss.2016.08.046

Brion N, Andersson M, Elskens M, Diaconu C, Baeyens W, Dehairs F, Middelburg J (2008) Nitrogen cycling, retention and export in a eutrophic temperate macrotidal estuary. Mar Ecol Prog Ser 357:87–99

Burchard H, Schuttelaars HM, Ralston DK (2018) Sediment trapping in estuaries. Annu Rev Mar Sci 10:371–395. https://doi.org/10.1146/annurev-marine-010816-060535

Cao W, Hong H, Yue S (2005) Modelling agricultural nitrogen contributions to the Jiulong River estuary and coastal water. Glob Planet Change 47:111–121. https://doi.org/10.1016/j.gloplacha.2004.10.006

Chen N, Wu J, Hong H (2012) Effect of storm events on riverine nitrogen dynamics in a subtropical watershed, southeastern China. Sci Total Environ 431:357–365. https://doi.org/10.1016/j.scitotenv.2012.05.072

Chen Y, Chen G, Ye Y (2015) Coastal vegetation invasion increases greenhouse gas emission from wetland soils but also increases soil carbon accumulation. Sci Total Environ 526:19–28. https://doi.org/10.1016/j.scitotenv.2015.04.077

Chen G, Chen B, Yu D, Tam NFY, Ye Y, Chen S (2016) Soil greenhouse gas emissions reduce the contribution of mangrove plants to the atmospheric cooling effect. Environ Res Lett 11:124019

Chen N, Krom MD, Wu Y, Yu D, Hong H (2018a) Storm induced estuarine turbidity maxima and controls on nutrient fluxes across river-estuary-coast continuum. Sci Total Environ 628–629:1108–1120. https://doi.org/10.1016/j.scitotenv.2018.02.060

Chen Y, Chen N, Li Y, Hong H (2018b) Multi-timescale sediment responses across a human impacted river-estuary system. J Hydrol 560:160–172. https://doi.org/10.1016/j.jhydrol.2018.02.075

Cheng P, Mao J, Yu F, Chen N, Wang A, Xu F (2019) A numerical study of residual flow induced by eddy viscosity-shear covariance in a tidally energetic estuary. Estuar Coast Shelf Sci 230:106446. https://doi.org/10.1016/j.ecss.2019.106446

Cottrell MT, Ras J, Kirchman DL (2010) Bacteriochlorophyll and community structure of aerobic anoxygenic phototrophic bacteria in a particle-rich estuary. ISME J 4:945–954. https://doi.org/10.1038/ismej.2010.13

Dai M, Wang L, Guo X, Zhai W, Li Q, He B, Kao SJ (2008) Nitrification and inorganic nitrogen distribution in a large perturbed river/estuarine system: the Pearl River Estuary, China. Biogeosciences 5:1227–1244

Damashek J, Francis CA (2018) Microbial nitrogen cycling in estuaries: from genes to ecosystem processes. Estuaries Coasts 41:626–660. https://doi.org/10.1007/s12237-017-0306-2

Damashek J, Casciotti K, Francis C (2016) Variable nitrification rates across environmental gradients in turbid, nutrient-rich estuary waters of San Francisco Bay. Estuaries Coasts 39:1050–1071. https://doi.org/10.1007/s12237-016-0071-7

Dettmann EH (2001) Effect of water residence time on annual export and denitrification of nitrogen in estuaries: a model analysis. Estuaries 24:481–490. https://doi.org/10.2307/1353250

DiLorenzo JL, Filadelfo RJ, Surak CR, Litwack HS, Gunawardana VK, Najarian TO (2004) Tidal variability in the water quality of an urbanized estuary. Estuaries 27:851–860. https://doi.org/10.1007/bf02912046

Doxaran D, Froidefond JM, Castaing P, Babin M (2009) Dynamics of the turbidity maximum zone in a macrotidal estuary (the Gironde, France): observations from field and MODIS satellite data. Estuar Coast Shelf Sci 81:321–332. https://doi.org/10.1016/j.ecss.2008.11.013

Erler DV, Santos IR, Zhang Y, Tait DR, Befus KM, Hidden A, Li L, Eyre BD (2014) Nitrogen transformations within a tropical subterranean estuary. Mar Chem 164:38–47. https://doi.org/10.1016/j.marchem.2014.05.008

Frame CH, Deal E, Nevison CD, Casciotti KL (2014) N_2O production in the eastern South Atlantic: analysis of N_2O stable isotopic and concentration data. Glob Biogeochem Cycles 28:1262–1278. https://doi.org/10.1002/2013gb004790

Glibert P, McCarthy J (1984) Uptake and assimilation of ammonium and nitrate by phytoplankton: indices of nutritional status for natural assemblages. J Plankton Res 6:677–697. https://doi.org/10.1093/plankt/6.4.677

Goncalves C, Brogueira MJ, Nogueira M (2015) Tidal and spatial variability of nitrous oxide (N2O) in Sado estuary (Portugal). Estuar Coast Shelf Sci 167:466–474. https://doi.org/10.1016/j.ecss.2015.10.028

Guo W, Xia E, Han Y, Wu F, Li M, Wu Y (2005) Fluorescent characteristics of colored dissolved organic matter (CDOM) in the Jiulong River Estuary. Oceanologia et Limnologia Sinica 36:349–357

Hamilton DP, Douglas GB, Adeney JA, Radke LC (2006) Seasonal changes in major ions, nutrients and chlorophyll a at two sites in the Swan River estuary, Western Australia. Mar Freshw Res 57:803–815. https://doi.org/10.1071/mf05046

Hsu RT, Liu JT (2010) In-situ estimations of the density and porosity of flocs of varying sizes in a submarine canyon. Mar Geol 276:105–109. https://doi.org/10.1016/j.margeo.2010.07.003

Hudon C, Gagnon P, Rondeau M, Hébert S, Gilbert D, Hill B, Patoine M, Starr M (2017) Hydrological and biological processes modulate carbon, nitrogen and phosphorus flux from the St. Lawrence River to its estuary (Quebec, Canada). Biogeochemistry 135:251–276. https://doi.org/10.1007/s10533-017-0371-4

Jiang YW, Wai OWH (2005) Drying–wetting approach for 3D finite element sigma coordinate model for estuaries with large tidal flats. Adv Water Resour 28:779–792. https://doi.org/10.1016/j.advwatres.2005.02.004

Liu SM, Hong GH, Zhang J, Ye XW, Jiang XL (2009) Nutrient budgets for large Chinese estuaries. Biogeosciences 6:2245–2263. https://doi.org/10.5194/bg-6-2245-2009

Loder TC, Reichard RP (1981) The dynamics of conservative mixing in estuaries. Estuaries 4:64–69. https://doi.org/10.2307/1351543

Long AM, Sun LY, Shi RG, Zhou WH, Dang AC (2013) Saltwater intrusion induced by a complete neap tide and its effect on nutrients variation in the estuary of Pearl River, China. J Coast Res 29:1158–1168. https://doi.org/10.2112/jcoastres-d-12-00182.1

Long AM, Xie Q, Yu XY, Xiao HW, Zhou WH (2018) Nutrient exchange between sediments and overlying waters in the Modaomen Estuary (China) over a complete semidiurnal tide cycle: implications of saltwater intrusion. J Coast Res 34:1439–1448. https://doi.org/10.2112/jcoastres-d-17-00104.1

Luo Z, Qiu Z, Wei Q, Du Laing G, Zhao Y, Yan C (2014) Dynamics of ammonia-oxidizing archaea and bacteria in relation to nitrification along simulated dissolved oxygen gradient in sediment–water interface of the Jiulong river

estuarine wetland, China. Environ Earth Sci 72:2225–2237. https://doi.org/10.1007/s12665-014-3128-6

Ma J, Li PC, Chen ZY, Lin KN, Chen NW, Jiang YY, Chen JX, Huang BQ, Yuan DX (2018) Development of an integrated syringe-pump-based environmental-water analyzer (iSEA) and application of it for fully automated real-time determination of ammonium in fresh water. Anal Chem 90:6431–6435. https://doi.org/10.1021/acs.analchem.8b01490

Martin GD, Vijay JG, Laluraj CM, Madhu NV, Joseph T, Nair M, Gupta GVM, Balachandran KK (2008) Fresh water influence on nutrient stoichiometry in a tropical estuary, southwest coast of India. Appl Ecol Environ Res 6:57–64

McAnally WH, Friedrichs C, Hamilton D, Hayter E, Shrestha P, Rodriguez H, Sheremet A, Teeter A, Flu ATCM (2007) Management of fluid mud in estuaries, bays, and lakes. I: Present state of understanding on character and behavior. J Hydraul Eng ASCE 133:9–22. https://doi.org/10.1061/(asce)0733-9429(2007)133:1(9)

Middelburg JJ, Herman PMJ (2007) Organic matter processing in tidal estuaries. Mar Chem 106:127–147. https://doi.org/10.1016/j.marchem.2006.02.007

Miguel L (2018) Study on seasonal hydrology and biogeochemical variability in a tropical estuarine system, Central Mozambique Coast, Africa. Mar Pollut Bull 131:674–692. https://doi.org/10.1016/j.marpolbul.2018.04.071

Mortimer RJG, Krom MD, Watson PG, Frickers PE, Davey JT, Clifton RJ (1999) Sediment–water exchange of nutrients in the intertidal zone of the Humber Estuary, UK. Mar Pollut Bull 37:261–279. https://doi.org/10.1016/S0025-326X(99)00053-3

Naik H, Chen CTA (2008) Biogeochemical cycling in the Taiwan Strait. Estuar Coast Shelf Sci 78:603–612. https://doi.org/10.1016/j.ecss.2008.02.004

Nilsson P, Jansson M (2002) Hydrodynamic control of nitrogen and phosphorus turnover in an eutrophicated estuary in the Baltic. Water Res 36:4616–4626. https://doi.org/10.1016/s0043-1354(02)00171-9

Owens NJP (1986) Estuarine nitrification: a naturally occurring fluidized bed reaction? Estuar Coast Shelf Sci 22:31–44. https://doi.org/10.1016/0272-7714(86)90022-3

Paudel B, Montagna PA (2014) Modeling inorganic nutrient distributions among hydrologic gradients using multivariate approaches. Ecol Inform 24:35–46. https://doi.org/10.1016/j.ecoinf.2014.06.003

Percuoco VP, Kalnejais LH, Officer LV (2015) Nutrient release from the sediments of the Great Bay Estuary, NH USA. Estuar Coast Shelf Sci 161:76–87. https://doi.org/10.1016/j.ecss.2015.04.006

Reef R, Feller IC, Lovelock CE (2010) Nutrition of mangroves. Tree Physiol 30:1148–1160. https://doi.org/10.1093/treephys/tpq048

Ribas-Ribas M, Anfuso E, Gomez-Parra A, Forja JM (2013) Tidal and seasonal carbon and nutrient dynamics of the Guadalquivir estuary and the Bay of Cadiz (SW Iberian Peninsula). Biogeosciences 10:4481–4491. https://doi.org/10.5194/bg-10-4481-2013

Rysgaard S, Thastum P, Dalsgaard T, Christensen PB, Sloth NP (1999) Effects of salinity on NH_4^+ adsorption capacity, nitrification, and denitrification in Danish estuarine sediments. Estuaries 22:21–30. https://doi.org/10.2307/1352923

Santos IR, Eyre BD, Huettel M (2012) The driving forces of porewater and groundwater flow in permeable coastal sediments: a review. Estuar Coast Shelf Sci 98:1–15. https://doi.org/10.1016/j.ecss.2011.10.024

Schaefert SC, Hollibaugh JT (2017) Temperature decouples ammonium and nitrite oxidation in coastal waters. Environ Sci Technol 51:3157–3164. https://doi.org/10.1021/acs.est.6b03483

Schlarbaum T, Daehnke K, Emeis K (2010) Turnover of combined dissolved organic nitrogen and ammonium in the Elbe estuary/NW Europe: results of nitrogen isotope investigations. Mar Chem 119:91–107. https://doi.org/10.1016/j.marchem.2009.12.007

Scully ME, Friedrichs CT (2007) Sediment pumping by tidal asymmetry in a partially mixed estuary. J Geophys Res Oceans 112:C07028. https://doi.org/10.1029/2006jc003784

Seitzinger S, Harrison JA, Bohlke JK, Bouwman AF, Lowrance R, Peterson B, Tobias C, Van Drecht G (2006) Denitrification across landscapes and waterscapes: a synthesis. Ecol Appl 16:2064–2090. https://doi.org/10.1890/1051-0761(2006)016[2064:dalawa]2.0.co;2

Seitzinger SP, Mayorga E, Bouwman AF, Kroeze C, Beusen AHW, Billen G, Van Drecht G, Dumont E, Fekete BM, Garnier J, Harrison JA (2010) Global river nutrient export: a scenario analysis of past and future trends. Global Biogeochem Cycles 24:GB0A08. https://doi.org/10.1029/2009GB003587

Smith MW, Allen LZ, Allen AE, Herfort L, Simon HM (2013) Contrasting genornic properties of free-living and particle-attached microbial assemblages within a coastal ecosystem. Front Microbiol 4:1–20. https://doi.org/10.3389/fmicb.2013.00120

Statham PJ (2012) Nutrients in estuaries—an overview and the potential impacts of climate change. Sci Total Environ 434:213–227. https://doi.org/10.1016/j.scitotenv.2011.09.088

Struyf E, Van Damme S, Meire P (2004) Possible effects of climate change on estuarine nutrient fluxes: a case study in the highly nutrified Schelde estuary (Belgium, The Netherlands). Estuar Coast Shelf Sci 60:649–661. https://doi.org/10.1016/j.ecss.2004.03.004

Tay HW, Bryan KR, Pilditch CA, Park S, Hamilton DP (2012) Variations in nutrient concentrations at different time scales in two shallow tidally dominated estuaries. Mar Freshw Res 63:95–109. https://doi.org/10.1071/MF11102

Tuduri A, Bergamino L, Violante R, Cavallotto JL, Garcia-Rodriguez F (2018) Spatial and temporal variation in the present and historical sedimentary organic matter within the Rio de la Plata estuary (South America) in relation to the salinity/turbidity gradient. J Sediment Environ 3:265–279. https://doi.org/10.12957/jse.2018.39152

Turner A, Millward GE (2002) Suspended particles: their role in estuarine biogeochemical cycles. Estuar Coast Shelf Sci 55:857–883. https://doi.org/10.1006/ecss.2002.1033

Uncles RJ, Stephens JA, Smith RE (2002) The dependence of estuarine turbidity on tidal intrusion length, tidal range and residence time. Cont Shelf Res 22:1835–1856. https://doi.org/10.1016/S0278-4343(02)00041-9

Uncles R, Stephens J, Harris C (2006) Properties of suspended sediment in the estuarine turbidity maximum of the highly turbid Humber Estuary system, UK. Ocean Dyn 56:235–247. https://doi.org/10.1007/s10236-005-0053-y

Vorosmarty CJ, Loder TC (1994) Spring neap tidal contrasts and nutrient dynamics in a marsh-dominated estuary. Estuaries 17:537–551. https://doi.org/10.2307/1352402

Wang F, Chen N, Yan J, Lin J, Guo W, Cheng P, Liu Q, Huang B, Tian Y (2019) Major Processes shaping mangroves as inorganic nitrogen sources or sinks: insights from a multidisciplinary study. J Geophys Res Biogeosci 124:1194–1208. https://doi.org/10.1029/2018jg004875

Wilson AM, Morris JT (2012) The influence of tidal forcing on groundwater flow and nutrient exchange in a salt marsh-dominated estuary. Biogeochemistry 108:27–38. https://doi.org/10.1007/s10533-010-9570-y

Wu Y (2015) Riverine nutrients export and its biogeochemical behavior in the Jiulong Estuary under subtropical storm events. Master Dissertation, Xiamen University

Wu J, Chen N, Hong H, Lu T, Wang L, Chen Z (2013) Direct measurement of dissolved N_2 and denitrification along a subtropical river-estuary gradient, China. Mar Pollut Bull 66:125–134. https://doi.org/10.1016/j.marpolbul.2014.05.016

Yan X, Zhai W, Hong H, Li Y, Guo W, Huang X (2012) Distribution, fluxes and decadal changes of nutrients in the Jiulong River Estuary, Southwest Taiwan Strait. Chin Sci Bull 57:2307–2318. https://doi.org/10.1007/s11434-012-5084-4

Yan XL, Wan XS, Liu L, Xu MN, Tan E, Zheng ZZ, Zou WB, Tian L, Li DW, Trull TW, Kao SJ (2019) Biogeochemical dynamics in a eutrophic tidal estuary revealed by isotopic compositions of multiple nitrogen species. J Geophys Res Biogeosci 124:1849–1864. https://doi.org/10.1029/2018jg004959

Yu D, Yan W, Chen N, Peng B, Hong H, Zhuo G (2015) Modeling increased riverine nitrogen export: source tracking and integrated watershed-coast management. Mar Pollut Bull 101:642–652. https://doi.org/10.1016/j.marpolbul.2015.10.035

Yu D, Chen NW, Krom MD, Lin JJ, Cheng P, Yu FL, Guo WD, Hong HS, Gao XJ (2019) Understanding how estuarine hydrology controls ammonium and other inorganic nitrogen concentrations and fluxes through the subtropical Jiulong River Estuary, SE China under baseflow and flood-affected conditions. Biogeochemistry 142:443–466. https://doi.org/10.1007/s10533-019-00546-9

Zakem EJ, Al-Haj A, Church MJ, van Dijken GL, Dutkiewicz S, Foster SQ, Fulweiler RW, Mills MM, Follows MJ (2018) Ecological control of nitrite in the upper ocean. Nat Commun 9:13. https://doi.org/10.1038/s41467-018-03553-w